Brownian motion as a new probe of wettability

Jianyong Mo, Akarsh Simha, and Mark G. Raizen

Citation: The Journal of Chemical Physics **146**, 134707 (2017); doi: 10.1063/1.4979177
View online: http://dx.doi.org/10.1063/1.4979177
View Table of Contents: http://aip.scitation.org/toc/jcp/146/13
Published by the American Institute of Physics

Brownian motion as a new probe of wettability

Jianyong Mo, Akarsh Simha, and Mark G. Raizen[a)]
Center for Nonlinear Dynamics and Department of Physics, The University of Texas at Austin, Austin, Texas 78712, USA

(Received 14 December 2016; accepted 13 March 2017; published online 7 April 2017)

Understanding wettability is crucial for optimizing oil recovery, semiconductor manufacturing, pharmaceutical industry, and electrowetting. In this letter, we study the effects of wettability on Brownian motion. We consider the cases of a sphere in an unbounded fluid medium, as well as a sphere placed in the vicinity of a plane wall. For the first case, we show the effects of wettability on the statistical properties of the particles' motion, such as velocity autocorrelation, velocity, and thermal force power spectra over a large range of time scales. We also propose a new method to measure wettability based on the particles' Brownian motion. In addition, we compare the boundary effects on Brownian motion imposed by both no-slip and perfect-slip flat walls. We emphasize the surprising boundary effects on Brownian motion imposed by a perfect-slip wall in the parallel direction, such as a higher particle mobility parallel to a perfect flat wall compared to that in the absence of the wall, as well as compared to a particle near a no-slip flat wall. *Published by AIP Publishing.* [http://dx.doi.org/10.1063/1.4979177]

I. INTRODUCTION

Wettability plays an important role in many situations, such as the self-cleaning mechanism of the lotus leaf due to its low wettability and waxing cars to protect them from rust. In industry, wettability plays a key role for optimizing oil recovery,[1] semiconductor manufacturing,[2] pharmaceutical industry,[3] and electrowetting.[4] The manufacture and characterization of materials of different wettabilities are thus of immense practical importance.

In addition, surface wettability can have a huge impact on Brownian motion. For example, it is well known that the magnitude of the steady Stokes drag force on a sphere of radius a moving at velocity v in a fluid with viscosity η is reduced from $F_s = 6\pi\eta av$ in the conventional case of a no-slip boundary condition to $F_s = 4\pi\eta av$ if the sphere has a perfect-slip boundary condition.[5]

Wettability, or slippage, is usually quantified in terms of an extrapolation length, the so-called slip length. The slip length δ is defined as the distance inside the solid wall where the linearly extrapolated fluid flow profile vanishes. The three boundary conditions are illustrated in Fig. 1. Figure 1(a) shows the case of the no-slip boundary condition, $\delta = 0$; Fig. 1(b) shows the case of a partial-slip boundary condition, where δ is finite; and Fig. 1(c) shows the case of the perfect-slip boundary condition, where $\delta = \infty$. The slip boundary condition can also be characterized by the contact angle θ_c, which in many cases is related to the slip length through $\delta = \delta_0(1 + \cos\theta_c)^{-2}$, where δ_0 is an empirical quasi-universal length scale and typically obtained from experiments.[6,7]

In fluid dynamics, the no-slip boundary condition is a conventional assumption at a fluid-solid interface, meaning that the fluid particles along the interface have zero velocity with respect to the solid surface. At macroscopic scales, the no-slip boundary condition is generally valid because in most cases the adhesive forces between the fluid molecules and solid particles are greater than the cohesive forces between the fluid molecules. This force imbalance brings down the fluid velocity to zero relative to the solid surface. Previous work[8,9] has shown that the assumption of no-slip boundary conditions on glass-water and glass-acetone interfaces is consistent with experiment. This is because the contact angle between water and glass (as well as acetone and glass) typically lies in the range 20° to 30°, resulting in a slip length of about 0.1 nm.[6,7] The diameters of particles used were about 10^4 times larger than the slip length, whereby the interface between water and micron-sized glass particles can be approximated with the no-slip boundary condition. We will show that this is a good assumption in Section III.

However, hydrophobic (and superhydrophobic if contact angle $\theta_c \geq 150°$) surfaces with slip lengths ranging from nanometers to even micrometers have been reported, showing that the no-slip assumption is insufficient and the partial-slip boundary condition must be used.[7,10–18] The two key features of superhydrophobic surfaces are low surface energy and micro- or nano-roughness typical with certain patterns, often called the lotus leaf structure.[6] The combination of surface roughness and hydrophobicity can trap an air layer in the depressions on the surface and result in the formation of an air-water interface that is supported by the peaks in the surface roughness. Therefore, the effective slip length can be increased significantly. In addition, the slip length can be increased by coating a hydrophobic self-assembled monolayer on the solid surface.[18] Glass microspheres with a partial-slip or even a near perfect-slip boundary condition can be created.

In this letter, we analyze the effects of wettability on Brownian motion in two systems: an unbounded spherical

a)Electronic mail: raizen@physics.utexas.edu

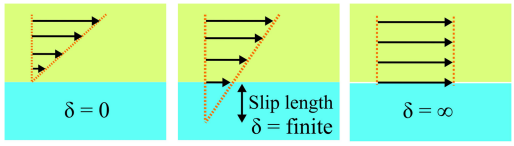

(A) No slip (B) Partial slip (C) Perfect slip

FIG. 1. Fluid flow boundary conditions at solid-fluid interfaces: (a) no slip, $\delta = 0$; (b) partial slip, δ is finite; (c) perfect slip, $\delta = \infty$. The light blue block represents the solid, the light green area indicates the fluid, and black arrows represent the fluid flow profile in the vicinity of the interface.

particle with different wettability conditions at its surface, leading to a proposal for a new method of wettability measurement; and a no-slip sphere bounded by a flat wall, which may offer either no-slip or perfect-slip boundary conditions. This paper is organized as follows. In Section II, we review the theory of Brownian motion of an unbounded particle with the arbitrary wettability condition and that for a no-slip sphere near a perfect-slip flat wall. In Section III, we give the numerical results for some statistical properties of Brownian motion and propose our new method of measuring wettability. In Section IV, we give numerical results comparing the boundary effects imposed on Brownian motion by both no-slip and perfect-slip flat walls. We conclude with a discussion in Section V.

II. THEORY

A. Hydrodynamic theory of Brownian motion

The position $\mathbf{x}(t)$ and velocity $\mathbf{v}(t)$ of a Brownian particle in equilibrium may be regarded as stationary and ergodic random processes. In all cases that we consider in this work (including the presence of a flat boundary), the Brownian motion in the three spatial directions decouples, whereby it is possible to consider each dimension separately. Thus, for simplicity of analysis, we shall consider the motion in any one direction, described by $x(t)$ and $v(t)$ in the following.

The position auto-correlation function (PACF) of the particle is defined through $C_x(t) \equiv \langle x(t+\tau)x(\tau)\rangle$. The mean square displacement (MSD) of the particle is defined as $\mathrm{MSD}(t) \equiv \left\langle [x(t+\tau) - x(\tau)]^2 \right\rangle$. The velocity auto-correlation function (VACF) of the particle is defined through $C_v(t) \equiv \langle v(t+\tau)v(\tau)\rangle$. The parentheses $\langle\ \rangle$ denote equilibrium ensemble averages, which may be reinterpreted as time averages through the assumption of ergodicity.

In the hydrodynamic theory of Brownian motion,[19–22] the Green-Kubo formula is used to relate these statistical properties to the admittance of the particle coupled to the fluid, which is the linear velocity response of the particle to an applied external force and defined as

$$\mathcal{Y}(\omega) = \frac{\tilde{v}(\omega)}{\tilde{E}(\omega)}, \tag{1}$$

where $\tilde{v}(\omega)$ and $\tilde{E}(\omega)$ are the Fourier transforms of the velocity of the particle and the applied force, respectively.

By the application of the Green-Kubo formula, equivalently the fluctuation-dissipation theorem, the velocity autocorrelation function $C_v(t)$ is related to the frequency-dependent admittance[20] through

$$\mathcal{Y}(\omega) = \frac{1}{k_B T}\int_0^\infty \mathrm{d}t\, e^{i\omega t} C_v(t), \tag{2}$$

where k_B is the Boltzmann's constant and T is the absolute temperature.

The Wiener-Khinchin theorem[23] states that the power spectral density (PSD) $S_\epsilon(\omega)$ of a stationary random process $\epsilon(t)$ and its autocorrelation function are Fourier transform pairs. Combining the Wiener-Khinchin theorem and the Green-Kubo formula Eq. (2), the position power spectral density (PSD) and velocity power spectral density (VPSD) can also be calculated from the admittance using[21]

$$S_x(\omega) = \frac{2k_B T\, \Re[\mathcal{Y}(\omega)]}{\omega^2} \tag{3}$$

and

$$S_v(\omega) = 2k_B T\, \Re[\mathcal{Y}(\omega)], \tag{4}$$

where $\Re$ denotes the real part. Through the Wiener-Khinchin theorem, the velocity autocorrelation function $C_v(t)$ and position autocorrelation function $C_x(t)$ can be obtained from their corresponding power spectra

$$\begin{aligned} C_v(t) &= \int_{-\infty}^{\infty} e^{-i\omega t} S_v(\omega)\mathrm{d}\omega/(2\pi) \\ &= 2k_B T \int_{-\infty}^{\infty} e^{-i\omega t}\Re[\mathcal{Y}(\omega)]\mathrm{d}\omega/(2\pi), \end{aligned} \tag{5}$$

$$\begin{aligned} C_x(t) &= \int_{-\infty}^{\infty} e^{-i\omega t} S_x(\omega)\mathrm{d}\omega/(2\pi) \\ &= 2k_B T \int_{-\infty}^{\infty} e^{-i\omega t}\frac{\Re[\mathcal{Y}(\omega)]}{\omega^2}\mathrm{d}\omega/(2\pi). \end{aligned} \tag{6}$$

Furthermore, the mean square displacement (MSD) of the particle can be found from the position autocorrelation function $C_x(t)$ via the identity

$$\langle \Delta x^2(t)\rangle = \langle [x(t_0+t) - x(t_0)]^2\rangle = 2\langle x(t)^2\rangle - 2C_x(t). \tag{7}$$

Alternatively, we may describe the Brownian motion $x(t)$ of the particle using a Generalized Langevin Equation (GLE). For a Brownian particle of mass m_p subject to a harmonic restoring force of stiffness K and frequency-dependent friction coefficient $\gamma(\omega)$, we may write the Fourier-transformed form of the GLE as

$$\left[-m_p\omega^2 - i\omega\gamma(\omega) + K\right]\tilde{x}(\omega) = \tilde{F}(\omega), \tag{8}$$

where $\tilde{x}(\omega)$ is the Fourier transform of $x(t)$ and $\tilde{F}(\omega)$ is the thermal force,[24,25] a random force that represents the effect of thermal fluctuations in the medium acting on the particle.

The thermal force power spectral density (FPSD, one-sided) acting on the particle can be obtained as[9,22]

$$S_F(\omega) = 4\pi k_B T \Re[\gamma(\omega)]. \tag{9}$$

Later, it will be shown that the drag coefficient $\gamma(\omega)$ is directly related to the admittance. Therefore, if the admittance of the particle's velocity $\mathcal{Y}(\omega)$ in the system of interest is known, the statistical properties of Brownian motion can be at least numerically obtained.

B. Theory of Brownian motion of an unbounded sphere with arbitrary wettability

The frequency dependent friction coefficient of a sphere in a liquid with an arbitrary wettability condition has been studied.[26] For a sphere of radius a offering a surface with a slip-length δ, oscillating with an angular frequency ω in a fluid of dynamic viscosity η, and density ρ_f, the friction coefficient is given by

$$\gamma_\delta(\omega) = \frac{2\pi\eta a}{3}\frac{(1+2\tilde{\delta})(9+9\tilde{\alpha}+\tilde{\alpha}^2)+\tilde{\delta}\tilde{\alpha}^2(1+\tilde{\alpha})}{1+(3+\tilde{\alpha})\tilde{\delta}}, \quad (10)$$

where the dimensionless quantities $\tilde{\alpha} = \sqrt{-i\omega\tau_f}$ ($\Re[\tilde{\alpha}] > 0$), $\tilde{\delta} = \delta/a$, and $\tau_f = \frac{\rho_f a^2}{\eta}$ is the time for the vorticity in the fluid to travel one sphere radius.[24]

In the case of a no-slip boundary condition, namely, $\delta = 0$, $\gamma_\delta(\omega)$ reduces to the well known frequency dependent friction coefficient of a no-slip sphere $\gamma_{\delta\to 0}(\omega) = \gamma_s(1+\tilde{\alpha}+\tilde{\alpha}^2/9)$,[24,25] where $\gamma_s = 6\pi\eta a$. The steady drag coefficient reduces to the well known result $\gamma_{\delta\to 0}(\omega = 0) = 6\pi\eta a$, as $\tilde{\alpha} \to 0$. As discussed in Section I, the slip length of water and acetone on conventional glass surfaces is about 0.1 nm, which is about 10^{-4} of the particle radius $a \sim 1$ μm, meaning $\tilde{\delta} \sim 10^{-4}$. The first-order correction in $\tilde{\delta}$ to the no-slip drag coefficient takes the form $-6\pi\eta a(1+\tilde{\alpha})^2\tilde{\delta}$ and is negligible compared to $\gamma_{\delta\to 0}(\omega)$ for all values of ω when $\tilde{\delta} \sim 10^{-4}$. Therefore, the no-slip boundary condition is a good assumption for those systems.

In the perfect-slip limit, namely, as $\delta \to \infty$, $\gamma_\delta(\omega)$ reduces to

$$\gamma_{\delta\to\infty}(\omega) = 6\pi\eta a\frac{2+2\tilde{\alpha}+\tilde{\alpha}^2/3+\tilde{\alpha}^3/9}{3+\tilde{\alpha}}. \quad (11)$$

The steady drag coefficient reduces to the well known result[5] $\gamma_{\delta\to\infty}(\omega = 0) = 4\pi\eta a$, as $\tilde{\alpha} \to 0$.

The admittance of a harmonically trapped sphere in a liquid with an arbitrary wettability condition can be obtained from the frequency-dependent friction coefficient through[8,9,25]

$$\mathcal{Y}_\delta(\omega) = \frac{1}{-i\omega m_p + \gamma_\delta(\omega) + \frac{K}{-i\omega}}, \quad (12)$$

where m_p is the sphere mass and K is the trapping strength of the harmonic trap.

C. Theory of Brownian motion of a no-slip sphere near a perfect-slip wall

We have reported the effects imposed on the Brownian motion of a microsphere by a much larger cylindrical glass wall, which approximates an idealized no-slip infinite flat wall.[9] In this section, we will discuss theoretical predictions for the boundary effects on the Brownian motion of a no-slip microsphere imposed by a perfect-slip infinite flat wall.

The theory for Brownian motion in such a system can be obtained similarly to the one presented in our previous work.[9,22] Whereas, the reaction field tensors in this system are different than that for a no-slip wall and have been given by Felderhof.[27,28] The reaction field tensor element for motion parallel to the wall is

$$R_\parallel^{\delta\to\infty}(h,\omega) = \frac{-1}{32\pi\eta h\nu^2}\left[1-(1+2\nu+4\nu^2)e^{-2\nu}\right] \quad (13)$$

and in the perpendicular direction is given by

$$R_\perp^{\delta\to\infty}(h,\omega) = \frac{-1}{16\pi\eta h\nu^2}\left[1-(1+2\nu)e^{-2\nu}\right], \quad (14)$$

where h is the distance between the center of the sphere and the wall, $\nu \equiv \sqrt{-i\omega\rho_f h^2/\eta} = \sqrt{-i\omega\tau_w}$, and τ_w is the time taken for vorticity in the fluid to traverse the distance from the wall to the sphere.

Furthermore, we may obtain the admittance of a no-slip particle near a perfect-slip flat wall for both directions in a similar manner, as[9,22]

$$\mathcal{Y}^\perp_{\delta\to\infty}(\omega) = \frac{1+\gamma_s(1+\tilde{\alpha}+\tilde{\alpha}^2/3)R_\perp^{\delta\to\infty}(h,\omega)}{(\gamma_0(\omega)-i\omega m_p)+i\omega(m_f-m_p)\gamma_s(1+\tilde{\alpha}+\tilde{\alpha}^2/3)R_\perp^{\delta\to\infty}(h,\omega)}, \quad (15)$$

$$\mathcal{Y}^\parallel_{\delta\to\infty}(\omega) = \frac{1+\gamma_s(1+\tilde{\alpha}+\tilde{\alpha}^2/3)R_\parallel^{\delta\to\infty}(h,\omega)}{(\gamma_0(\omega)-i\omega m_p)+i\omega(m_f-m_p)\gamma_s(1+\tilde{\alpha}+\tilde{\alpha}^2/3)R_\parallel^{\delta\to\infty}(h,\omega)}, \quad (16)$$

where m_p is the particle mass, m_f is the mass of the fluid displaced by the sphere, and $\gamma_0(\omega) \equiv \gamma_s(1+\tilde{\alpha}+\tilde{\alpha}^2/9)$.

The effective masses of the particle near a flat wall in perpendicular and parallel directions become[9,22,29,30]

$$m^*_\perp = m_p + \frac{1}{2}m_f\left(1+\frac{3}{8}\left(\frac{a}{h}\right)^3\right), \quad (17)$$

$$m^*_\parallel = m_p + \frac{1}{2}m_f\left(1+\frac{3}{16}\left(\frac{a}{h}\right)^3\right). \quad (18)$$

It is worth emphasizing that the effective masses $m^*_\perp$ and $m^*_\parallel$ do not depend on the wettability condition on the wall. According to the modified energy equipartition theorem,[31] the velocity variance becomes anisotropic as well and is

$$\langle(v^*_\parallel)^2\rangle = \frac{k_BT}{m^*_\parallel}, \quad (19)$$

$$\langle(v^*_\perp)^2\rangle = \frac{k_BT}{m^*_\perp} \quad (20)$$

in the parallel and perpendicular directions, respectively. The apparent conflict with the equipartition theorem can be resolved by considering the effects of compressibility of the

liquid.[31] Below time scales on the order of $\tau_c = a/c$, where c is the speed of sound in the liquid and a is the radius of the sphere, the compressibility of the liquid cannot be neglected and the velocity variance will approach the energy equipartition theorem.

III. BROWNIAN MOTION OF AN UNBOUNDED MICROSPHERE WITH DIFFERENT WETTABILITY CONDITIONS

In this section, we give numerical predictions for the Brownian motion of a harmonically trapped microsphere with arbitrary wettability conditions in water ($\rho_f = 1$ g/cm^3, $\eta = 0.9 \times 10^{-3}$ Pa s). The sphere has a diameter of 3 μm and a density of 2 g/cm^3. The trap strength used in this numerical study is $K = 150$ μN/m, which is typical in previous experimental work.[8,9,25] As discussed in Section II, once the admittance of the particle is obtained using Eq. (12), the statistical properties of the particle's Brownian motion can be calculated through Eqs. (3)–(9).

A. Mean square displacement

The predictions for the mean square displacement of the particle with different boundary conditions on the particle's surface are shown in Fig. 2. At long time scales, the harmonic trap confines the particle and causes the MSD to plateau to the same value independent of the slippage. This value depends only on the trapping strength and the temperature and may be calculated by applying the equipartition theorem as $\frac{1}{2}K\langle\Delta x^2\rangle = \frac{1}{2}k_BT$. At short time scales, the slippage on the particle surface results in a reduced friction force on the particle. Therefore, the MSD increases more rapidly with increasing the slip length.

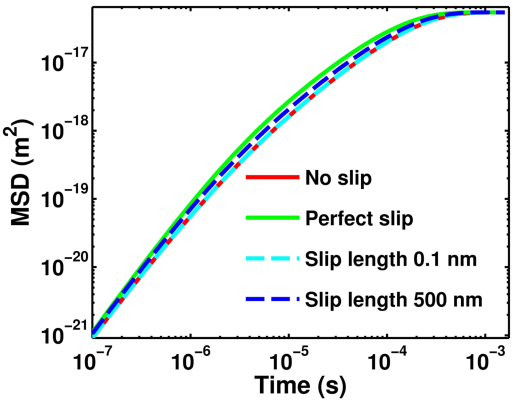

FIG. 2. The numerical predictions for the mean square displacements of an unbounded microsphere (3 μm in diameter, density of 2 g/cm^3) held by a harmonic trap ($K = 150$ μN/m) in a fluid with density $\rho_f = 1$ g/cm^3 and dynamic viscosity $\eta = 0.9 \times 10^{-3}$ Pa s with different surface wettability conditions.

B. Velocity autocorrelation function

The numerical predictions for the velocity autocorrelation function $C_v(t)$ (normalized to k_BT/m^*, where $m^* = (m_p + \frac{1}{2}m_f)$) with different boundary conditions on the sphere's surface are shown in Fig. 3. The red solid line represents the prediction for the VACF in the no-slip limit and the green solid line predicts the VACF in the perfect-slip limit. The dashed lines are the predictions with partial-slip boundary conditions. In particular, the agreement between the VACF with the no-slip boundary condition and the VACF with a slip length of 0.1 nm (the cyan dashed line) indicates that the interface between glass and water can indeed be assumed to be no-slip in experiments.[8,9]

With a larger slip length, the particle VACF decays less rapidly over time, owing to a lower dissipation rate. Measurements of the particle's instantaneous velocity are of great significance to test the tenets of statistical mechanics, such as the Maxwell-Boltzmann distribution.[8,25,32] To be ableat high frequencies causes the power to measure the instantaneous velocity of the particle, one needs to have a detection system with a temporal resolution that is high enough to measure the normalized VACF close to 1. Therefore, it is much easier to measure the particle's instantaneous velocity of a particle with a perfect-slip boundary, than with a no-slip boundary.

C. Velocity power spectral density

The predictions for the velocity power spectral density with different boundary conditions on the sphere's surface are shown in Fig. 4. With increasing the slip length, the power of the velocity is redistributed towards low frequencies, which facilitates precise measurements of the instantaneous velocity of a particle with large slip lengths. This may be explained in terms of the behavior of the thermal force (which we shall investigate in Sec. III D). At high frequencies, the thermal force grows asymptotically as $\sqrt{\omega}$ for the no-slip case, whereas this is suppressed by saturation to a constant value in the full-slip case. As a result of the area under the entire curve being held constant (at k_BT/m^*), the lowered

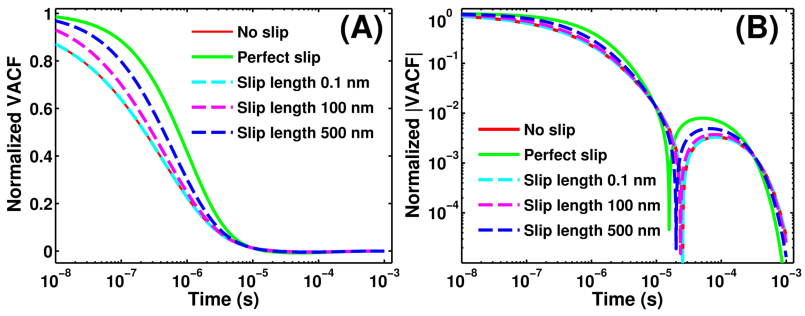

FIG. 3. The numerical predictions for the velocity autocorrelation functions (normalized to k_BT/m^*) of an unbounded microsphere (3 μm in diameter, density of 2 g/cm^3) in a fluid with density $\rho_f = 1$ g/cm^3 and dynamic viscosity $\eta = 0.9 \times 10^{-3}$ Pa s with different surface wettability conditions (a), on a log-linear plot; (b), the absolute value on a log-log scale. The cusps indicate zero crossings, which are a consequence of the presence of the harmonic trap ($K = 150$ μN/m).

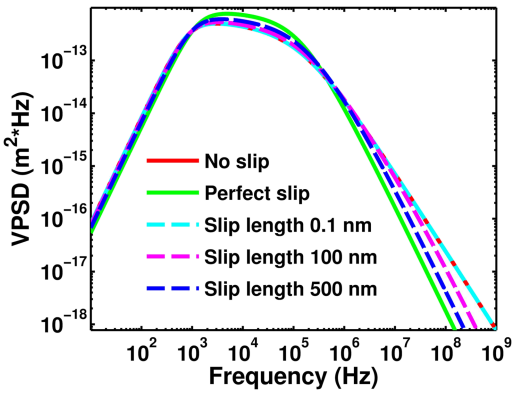

FIG. 4. The numerical predictions for the velocity power spectral densities of an unbounded microsphere (3 μm in diameter, density of 2 g/cm^3) held by a harmonic trap (K = 150 μN/m) in a fluid with density ρ_f = 1 g/cm^3 and dynamic viscosity $\eta = 0.9 \times 10^{-3}$ Pa s with different surface wettability conditions.

force at high frequencies causes the power to shift to lower frequencies.

D. Thermal force power spectral density

Figure 5 shows the predictions for the power spectral density of the thermal force on the sphere with different boundary conditions on the sphere's surface. The thermal force on the sphere with partial (and perfect) slip boundary conditions becomes less colored, as the thermal force PSD tends to flatten with increasing the slip length. Both the DC values of the thermal force spectrum and the drag force decrease with increasing the slip length, which is consistent with the fluctuation-dissipation theorem.[33] The high frequency behavior is significantly affected by the slippage on the particle's surface. The thermal force spectrum with slip boundary conditions no longer has an asymptotic dependence of $\sqrt{\omega}$ and instead tends towards saturation. In the perfect-slip limit, the thermal force at high frequencies saturates at

$$S_F(\omega \to \infty) \simeq 48\pi^2 \eta a k_B T \tag{21}$$

which is 3 times that of the corresponding DC value.

In summary, the sphere's surface wettability condition can drastically affect Brownian motion. Therefore, by measuring the particle's motion, we can extract the wettability of the fluid on the particle's surface. This can be accomplished in a manner similar to previous work by treating the slip length as one of the fitting parameters.[8,9,25] We will propose the detail of such an experiment in Section III E.

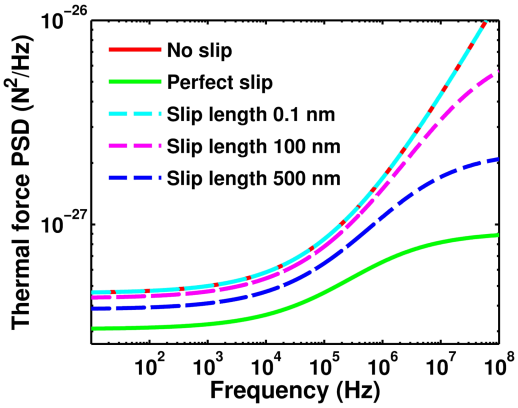

FIG. 5. The numerical predictions for the power spectral density of the thermal force on an unbounded microsphere (3 μm in diameter, density of 2 g/cm^3) in a fluid with density ρ_f = 1 g/cm^3 and dynamic viscosity $\eta = 0.9 \times 10^{-3}$ Pa s with different surface wettability conditions.

E. Experimental proposal of measuring wettability using Brownian motion

Wettability, as we have discussed, has a direct bearing on the drag experienced by a particle in a liquid, which in turn has a measurable impact on its Brownian motion. In this section, we propose an experiment to determine the wettability of the surface of a sphere in a given liquid by making precise measurements of its Brownian motion. The setup under consideration is similar to the setups used in previous experiments,[8,25] with some modifications, which we shall describe in greater detail here.

A schematic of such a setup is shown in Fig. 6. A pair of optical tweezers is constructed using a laser beam focused by a microscope objective of sufficiently high numerical aperture to trap a transparent spherical particle within a liquid chamber. The trapping beam after passing through the trapped particle is re-collimated by an identical objective and is then split into two roughly equal halves by a D-shaped mirror before being focused onto a high-bandwidth balanced detector. The trapped particle near the trapping laser focus scatters some of the incident photons in a direction which depends on the particle's position. Changes in the particle's position are encoded in the spatial distribution of the scattered laser beam, which can be measured with a high sensitivity using a balanced detection system. The result is a measurement of the projection of the particle's Brownian motion along one dimension, which is sufficient to determine the slip length δ of the fluid on the particle's surface.

The laser should be chosen such that both the fluid and the particle used have low absorption for its wavelength, since absorption of the laser by the liquid or the particle can cause local heating, leading to a non-equilibrium state.[34] Examples of fluids and particles that have been used in previous experiments include water, acetone and silica glass, barium titanate glass, and polystyrene. For these fluids and particles, some possible choices of laser wavelength include 532 nm and 1064 nm.

One of the major differences between the previous experiments and the proposed experiment lies in the wettability conditions on the particles' surface. Particles with large slip lengths on the surface can be created by two economical methods: one is by coating the glass surface with a superhydrophobic structure with nano-scale roughness,[35] which increases the effective slip length to the order of 100 nm; the other is to coat

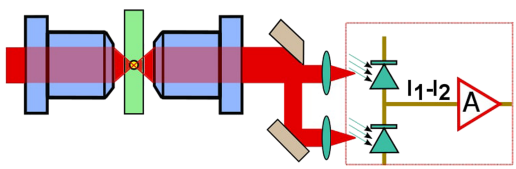

FIG. 6. A simplified schematic of an experimental setup for measuring wettability on a sphere's surface using Brownian motion.

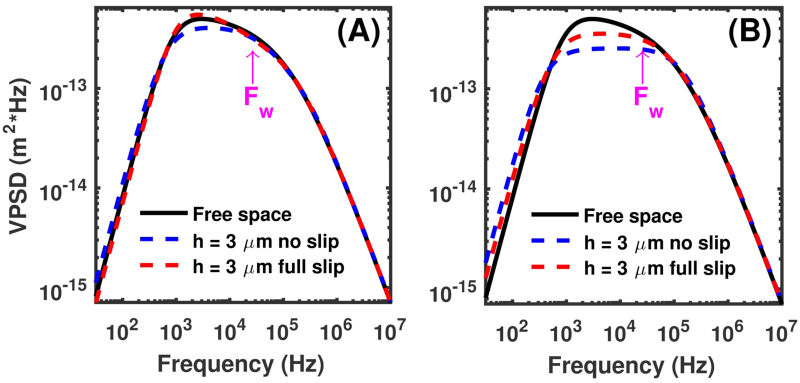

FIG. 7. The numerical predictions for the velocity power spectral density of a no-slip microsphere (3 μm in diameter, density of 2 g/cm^3) held by a harmonic trap (K = 150 μN/m) in a fluid with density ρ_f = 1 g/cm^3 and dynamic viscosity $\eta = 0.9\times10^{-3}$ Pa s in three cases: unbounded (free space, black line), 3 μm away from a flat infinite no-slip wall (blue dashed line), and 3 μm away from a flat infinite perfect-slip wall (red dashed line) (a) in the direction parallel to the wall and (b) in the direction perpendicular to the wall.

the glass with a self-assembled monolayer of phosphonates,[36] with which a slip length of larger than 10 nm can be achieved.

A high-bandwidth, high-gain, and low-noise lab-built balanced detector[25] may be used in this proposed experiment. The detector signal can be digitized and saved on a computer by a high-resolution, high-speed digitizer (~100 MHz, 200 MSa/s, such as GaGe Razor 1622). The position, velocity, and thermal force power spectra as well as the MSD and VACF can be numerically calculated from the acquired data.[8,25,37]

Among those statistical quantities, we consider the VACF to be the statistic of choice for fitting because it is less sensitive to noise and shows significant variation with different slip lengths. In our previous work, we have shown that the VACF is the best statistic to determine the distance to a boundary for similar reasons.[9] It is however easy to try out various statistics and see which ones give the most reliable results.

The experimentally obtained VACF is then fit to the theoretical VACF function, which is calculated numerically as described by Eq. (5). Least-squares fitting of the VACF can be performed to determine four fitting parameters: a calibration factor having units of V/m that defines the linear relationship between the measured voltage and the displacement of the particle; the particle's radius a; the stiffness of the optical harmonic trap K; and the desired slip length δ.

IV. COMPARISON OF THE BOUNDARY EFFECTS ON BROWNIAN MOTION IMPOSED BY BOTH NO-SLIP AND PERFECT-SLIP FLAT WALLS

In this section, we will give the numerical predictions for a variety of statistical quantities for the Brownian motion of no-slip sphere in three cases: unbounded, near a no-slip flat infinite wall, and near a perfect-slip (full slip) flat infinite wall. These predictions will be used to study both boundary effects and wettability effects. The particle considered here is a 3 μm diameter silica sphere (ρ = 2.0 g/cm^3) trapped in water by a harmonic trap with a trap strength of 150 μN/m. In the cases with the wall, the sphere-wall separation is set to h = 3 μm. As pointed out in previous work,[9,22] the theory we use[20,27] works well when the ratio between the sphere radius and the sphere-wall separation a/h equals to or is smaller than 1/2. The admittance of the particle may be obtained using Eqs. (15) and (16), and as before, the statistical properties of the particle's Brownian motion can be calculated using Eqs. (3)–(9).

A. Velocity power spectral density

The predictions for the velocity power spectral density (VPSD) of the sphere in the three cases are shown in Fig. 7. At frequencies much higher than $F_w = 1/(2\pi\tau_w)$, the boundary effects imposed by both no-slip and perfect-slip walls are negligible. This is because it takes time τ_w for the vorticity in the fluid to traverse the distance from the wall to the center of the sphere. In the perpendicular direction, as shown in Fig. 7(b), the boundary effects imposed by the perfect-slip wall are similar to those imposed by the no-slip wall, which is due to the fact that the no penetration boundary condition holds for both no-slip and perfect-slip boundary conditions. However, they are qualitatively different in the parallel direction as shown in Fig. 7(a). Unlike the case of a no-slip wall, the parallel VPSD of the sphere near a perfect-slip wall is suppressed at low frequencies and enhanced at intermediate frequencies.

B. Mean square displacement

The predictions for the mean square displacement (MSD) of the sphere in the three cases are shown in Fig. 8. At long

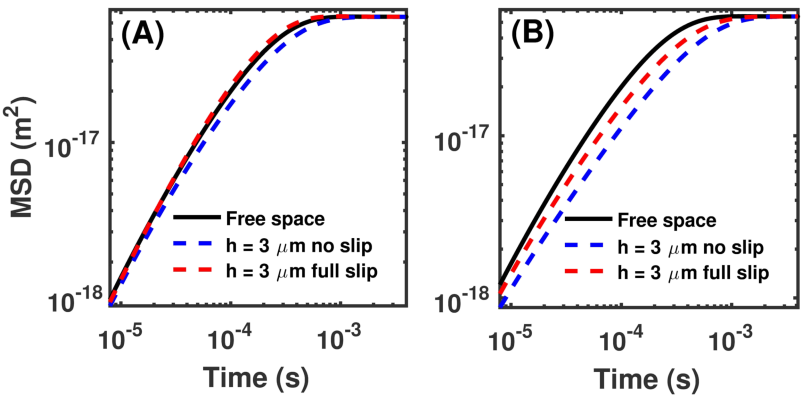

FIG. 8. The numerical predictions for the mean square displacements of a no-slip microsphere (3 μm in diameter, density of 2 g/cm^3) held by a harmonic trap (K = 150 μN/m) in a fluid with density ρ_f = 1 g/cm^3 and dynamic viscosity $\eta = 0.9\times10^{-3}$ Pa s in three cases: unbounded (free space, black line), 3 μm away from a flat infinite no-slip wall (blue dashed line), and 3 μm away from a flat infinite perfect-slip wall (red dashed line) (a) in the direction parallel to the wall and (b) in the direction perpendicular to the wall.

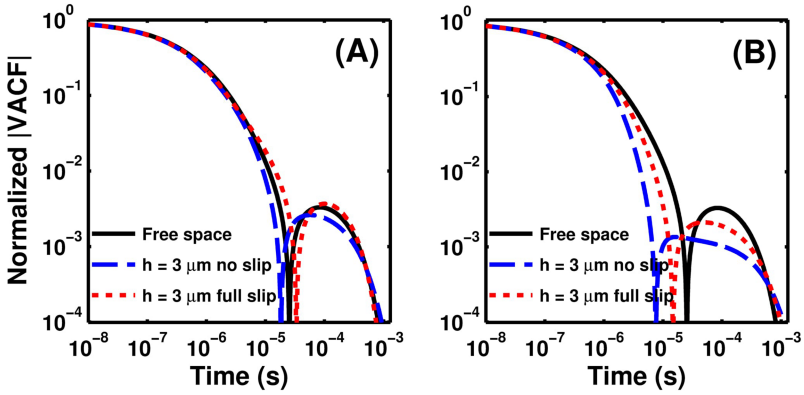

FIG. 9. The numerical predictions for the velocity autocorrelation function of a no-slip microsphere (3 μm in diameter, density of 2 g/cm^3) in a fluid with density ρ_f = 1 g/cm^3 and dynamic viscosity $\eta = 0.9\times10^{-3}$ Pa s in three cases: unbounded (free space, black line), 3 μm away from a flat infinite no-slip wall (blue dashed line), and 3 μm away from a flat infinite perfect-slip wall (red dashed line) (a) in the direction parallel to the wall and (b) in the direction perpendicular to the wall. The plots show the absolute value on a log-log scale, normalized to $\langle(v_\parallel^*)^2\rangle$ and $\langle(v_\perp^*)^2\rangle$ in the parallel and perpendicular directions, respectively. The cusps indicate zero crossings, which are a consequence of the presence of the harmonic trap (K = 150 μN/m).

time scales, the MSDs of each case in both parallel and perpendicular directions plateau to the same value due to confinement caused by the trap. As compared to the MSD of an unbounded particle, the MSDs of particle in the perpendicular direction to no-slip and perfect-slip walls are both suppressed, as shown in Fig. 8(b), implying that the sphere experiences a stronger drag force for motion perpendicular to a wall regardless of the boundary condition on the wall surface. However, the amount by which the drag force is strengthened depends on the boundary condition at the wall. In the parallel direction, however, there is also a qualitative dependence of the drag force on the wettability conditions on the surface of the wall. It is surprising that the MSD of the sphere in the parallel direction to the perfect-slip wall actually increases more rapidly as compared to that of an unbounded sphere, which means that the sphere experiences less drag force when moving in parallel to a perfect-slip wall as compared to that in the absence of the wall.

Here, we give the DC values of the drag coefficients of a sphere near a perfect-slip wall in both directions (to the first order in a/h),

$$\gamma^{\parallel}_{\delta\to\infty}(\omega=0) = 6\pi\eta a\frac{1}{1+\frac{3a}{8h}}, \tag{22}$$

$$\gamma^{\perp}_{\delta\to\infty}(\omega=0) = 6\pi\eta a\frac{1}{1-\frac{3a}{4h}}. \tag{23}$$

With these, the diffusion coefficients to first order in a/h in the two directions can be obtained using the Einstein-Stokes relation

$$\mathcal{D}^{\parallel}_{\delta\to\infty}(\omega=0) = \frac{k_BT}{6\pi\eta a}\left(1+\frac{3a}{8h}\right) = D_0\left(1+\frac{3a}{8h}\right), \tag{24}$$

$$\mathcal{D}^{\perp}_{\delta\to\infty}(\omega=0) = \frac{k_BT}{6\pi\eta a}\left(1-\frac{3a}{4h}\right) = D_0\left(1-\frac{3a}{4h}\right), \tag{25}$$

where $D_0 = \frac{k_BT}{6\pi\eta a}$ is the particle's diffusion coefficient in unbounded fluid. The diffusion coefficient $\mathcal{D}^{\parallel}_{\delta\to\infty}(\omega=0)$ is actually larger than D_0, meaning the particle has a higher mobility when closer to a perfect-slip wall. This surprising effect has been experimentally demonstrated for a sphere moving near a fluid-air interface, which can be considered to be nearly perfect-slip.[38]

C. Velocity autocorrelation function

The numerical predictions for the velocity autocorrelation function $C_v(t)$ of the sphere (normalized to $\langle(v_\parallel^*)^2\rangle$ and $\langle(v_\perp^*)^2\rangle$ in the parallel and perpendicular directions, respectively) in the three cases are shown in Fig. 9. In the perpendicular direction, the boundary effects imposed by both no-slip and perfect-slip walls cause a more rapid decay in the VACF as compared to that in the unbounded case, which is consistent with previous numerical simulations.[39,40] However, in the parallel direction, the VACF of a sphere near a perfect-slip wall initially decays faster than the one in the unbounded case, followed by a slower decay at intermediate time scales.

D. Thermal force power spectral density

The predictions for the power spectral density of the thermal force in the three cases are shown in Fig. 10. As

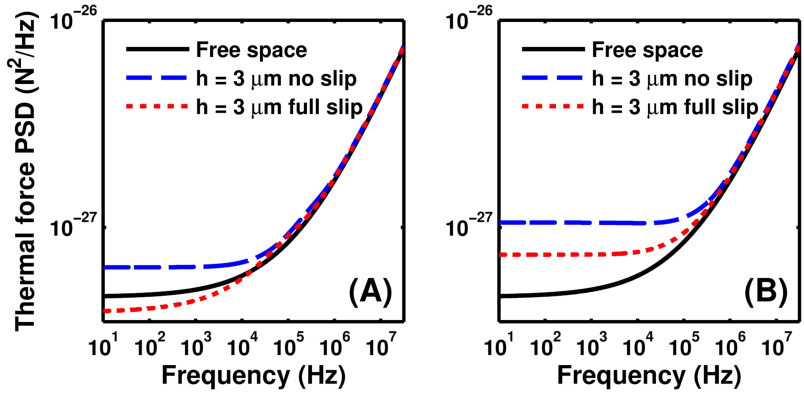

FIG. 10. The numerical predictions for the thermal force power spectra on a no-slip microsphere (3 μm in diameter, density of 2 g/cm^3) in a fluid with density ρ_f = 1 g/cm^3 and dynamic viscosity $\eta = 0.9\times10^{-3}$ Pa s in three cases: unbounded (free space, black line), 3 μm away from a flat infinite no-slip wall (blue dashed line), and 3 μm away from a flat infinite perfect-slip wall (red dashed line) (a) in the direction parallel to the wall and (b) in the direction perpendicular to the wall.

discussed in previous work,[9,22] the thermal force loses its color at low frequencies as the particle approaches a no-slip wall. The same holds true for motion perpendicular to a perfect-slip wall. However, the behavior is qualitatively different in the parallel direction. The thermal force in the parallel direction on a sphere near a perfect-slip wall does not lose its color.

The low frequency behavior of the thermal force near a perfect-slip wall can be understood by the asymptotic form of the thermal force PSD (one-sided) exerted on the particle as $\omega \to 0$, which is given (to the first order in a/h) in the parallel direction by

$$S_{F,\parallel}^{\delta\to\infty}(\omega) = 4k_BT\gamma_s\left(\frac{1}{1+\frac{3a}{8h}} + \frac{64\sqrt{2}h^2}{(8h+3a)^2}(\omega\tau_f)^{\frac{1}{2}}\right) \tag{26}$$

and in the perpendicular direction by

$$S_{F,\perp}^{\delta\to\infty}(\omega) = 4k_BT\gamma_s\left(\frac{1}{1-\frac{3a}{4h}} + \frac{8\sqrt{2}(6h^4-5a^2h^2)}{15a^2(4h-3a)^2}(\omega\tau_f)^{\frac{3}{2}}\right). \tag{27}$$

The DC values of $S_{F,\parallel}^{\delta\to\infty}$ and $S_{F,\perp}^{\delta\to\infty}$ change to $4k_BT\gamma_s\frac{1}{1+\frac{3a}{8h}}$ and $4k_BT\gamma_s\frac{1}{1-\frac{3a}{4h}}$ from the bulk value of $4k_BT\gamma_s$, respectively. The change in the thermal force is consistent with the change in the drag force, in accordance with the fluctuation-dissipation theorem.[33]

The flatness of the power spectral density of the thermal force on a sphere near a perfect-slip flat wall in the perpendicular direction can be understood in a manner akin to the no-slip wall case.[9,22] In contrast, this effect is not seen in the parallel direction in the case of a perfect-slip plane wall. This is observed in Eq. (26) through the presence of the leading term $(\omega\tau_f)^{\frac{1}{2}}$, in contrast with Eq. (27) where this leading term is absent. This is probably due to constructive interference from the reflected flow.

In summary, some conclusions drawn in previous work[9] still hold for the case of a sphere near a perfect-slip wall. For instance, boundary effects imposed by a perfect-slip flat wall occur at time scales longer than τ_w, equivalently, frequency scales lower than F_w. In the perpendicular direction, the boundary effects imposed by a perfect-slip wall are only quantitatively different from those caused by a no-slip wall, which can be ascribed to the no-penetration boundary condition remaining the same for both cases. With the same sphere-wall separation, the boundary effects in the perpendicular direction near a perfect-slip wall are weaker than those near a no-slip wall. However, in the parallel direction, the boundary effects caused by the two types of walls are qualitatively different. We expect that the boundary effects imposed by a partial-slip flat wall will manifest as a hybrid of the effects caused by a no-slip wall and a perfect-slip wall.

V. DISCUSSION

In this letter, we studied the effects of arbitrary wettability conditions on the sphere's surface on its Brownian motion. Our new proposed method for measuring wettability could be used in many applications, such as pharmaceutical development,[3] emulsions' preparation and stability,[41] and animal suspension-feeding.[42] In addition, we also compared the boundary effects on Brownian motion imposed by both no-slip and perfect-slip flat walls and pointed out the surprising boundary effects on Brownian motion imposed by a perfect-slip wall in the parallel direction.

Further avenues for research include an experimental study of the effects of wettability on Brownian motion. By coating the glass surface with a superhydrophobic structure with nano-scale roughness or with a self-assembled monolayer of phosphonates, we can achieve different wettability conditions with a slip length of up to a few hundred nm both on the sphere and the boundary wall.

ACKNOWLEDGMENTS

We acknowledge the support from the Sid W. Richardson Foundation and the R. A. Welch Foundation Grant No. F-1258. A.S. acknowledges support from the University of Texas at Austin Graduate Continuing Fellowship.

[1] N. R. Morrow, J. Pet. Technol. **42**, 1476 (1990).
[2] J. Wang, in *56th Electronic Components and Technology Conference 2006* (IEEE, 2006), pp. 467–473.
[3] D. Zhang, J. H. Flory, S. Panmai, U. Batra, and M. J. Kaufman, Colloids Surf., A **206**, 547 (2002).
[4] F. Mugele, A. Klingner, J. Buehrle, D. Steinhauser, and S. Herminghaus, J. Phys.: Condens. Matter **17**, S559 (2005).
[5] A. B. Basset, Philos. Trans. R. Soc., A **179**, 43 (1888).
[6] R. S. Voronov, D. V. Papavassiliou, and L. L. Lee, J. Chem. Phys. **124**, 204701 (2006).
[7] D. M. Huang, C. Sendner, D. Horinek, R. R. Netz, and L. Bocquet, Phys. Rev. Lett. **101**, 226101 (2008).
[8] J. Mo, A. Simha, S. Kheifets, and M. G. Raizen, Opt. Express **23**, 1888 (2015).
[9] J. Mo, A. Simha, and M. G. Raizen, Phys. Rev. E **92**, 062106 (2015).
[10] R. Pit, H. Hervet, and L. Léger, Phys. Rev. Lett. **85**, 980 (2000).
[11] V. S. J. Craig, C. Neto, and D. R. M. Williams, Phys. Rev. Lett. **87**, 054504 (2001).
[12] Y. Zhu and S. Granick, Phys. Rev. Lett. **87**, 096105 (2001).
[13] Z. Liang and P. Keblinski, J. Chem. Phys. **142**, 134701 (2015).
[14] P. Joseph, C. Cottin-Bizonne, J.-M. Benoît, C. Ybert, C. Journet, P. Tabeling, and L. Bocquet, Phys. Rev. Lett. **97**, 156104 (2006).
[15] C.-H. Choi, U. Ulmanella, J. Kim, C.-M. Ho, and C.-J. Kim, Phys. Fluids **18**, 087105 (2006).
[16] H. Ogihara, J. Xie, J. Okagaki, and T. Saji, Langmuir **28**, 4605 (2012).
[17] D. Song, R. J. Daniello, and J. P. Rothstein, Exp. Fluids **55**, 1783 (2014).
[18] M. Chinappi and C. M. Casciola, Phys. Fluids **22**, 042003 (2010).
[19] R. Zwanzig and M. Bixon, Phys. Rev. A **2**, 2005 (1970).
[20] B. U. Felderhof, J. Phys. Chem. B **109**, 21406 (2005).
[21] T. Franosch and S. Jeney, Phys. Rev. E **79**, 031402 (2009).
[22] A. Simha, J. Mo, and P. J. Morrison, "Unsteady stokes flow near boundaries: The point-particle approximation and the method of reflections" (unpublished).
[23] V. Balakrishnan, Pramana **12**, 301 (1979).
[24] T. Franosch, M. Grimm, M. Belushkin, F. M. Mor, G. Foffi, L. Forró, and S. Jeney, Nature **478**, 85 (2011).
[25] S. Kheifets, A. Simha, K. Melin, T. Li, and M. G. Raizen, Science **343**, 1493 (2014).
[26] A. Erbaş, R. Podgornik, and R. R. Netz, Eur. Phys. J. E **32**, 147 (2010).
[27] B. U. Felderhof, J. Chem. Phys. **136**, 144701 (2012).
[28] B. U. Felderhof, Phys. Rev. E **85**, 046303 (2012).
[29] H. Lamb, *Hydrodynamics* (University Press, 1916), p. 708.
[30] F.-L. Yang, Phys. Fluids **22**, 123303 (2010).
[31] R. Zwanzig and M. Bixon, J. Fluid Mech. **69**, 21 (1975).
[32] T. Li, S. Kheifets, D. Medellin, and M. G. Raizen, Science **328**, 1673 (2010).
[33] R. Kubo, Rep. Prog. Phys. **29**, 255 (1966).
[34] D. Rings, R. Schachoff, M. Selmke, F. Cichos, and K. Kroy, Phys. Rev. Lett. **105**, 090604 (2010).
[35] See http://lotusleaf.octochemstore.com/ for instance, HydroFoe coating.
[36] See http://www.aculon.com/samp-technology.php for example, Aculon.

[37]K. Berg-Sørensen and H. Flyvbjerg, Rev. Sci. Instrum. **75**, 594 (2004).
[38]G. M. Wang, R. Prabhakar, and E. M. Sevick, Phys. Rev. Lett. **103**, 248303 (2009).
[39]K. Huang and I. Szlufarska, Nat. Commun. **6**, 8558 (2015).
[40]H.-Y. Yu, D. M. Eckmann, P. S. Ayyaswamy, and R. Radhakrishnan, Phys. Rev. E **91**, 052303 (2015).
[41]S. Stiller, H. Gers-Barlag, M. Lergenmueller, F. Pflücker, J. Schulz, K. P. Wittern, and R. Daniels, Colloids Surf., A **232**, 261 (2004).
[42]S. Conova, Mar. Biol. **133**, 419 (1999).